Scaling the effects of surface topography in the secondary atomization resulting from droplet/wall interactions

Ana S. Moita[1], António L. N. Moreira[1]

1: Laboratory of Thermofluids, Combustion and Energy Systems at IN+, Technical University of Lisbon-Instituto Superior Técnico, Lisbon, Portugal, anamoita@dem.ist.utl.pt
2: Laboratory of Thermofluids, Combustion and Energy Systems at IN+, Technical University of Lisbon-Instituto Superior Técnico, Lisbon, Portugal, moreira@dem.ist.utl.pt

Abstract The present paper addresses the scaling of the effects of surface topography in the size of the secondary droplets generated by thermal induced atomization of single droplets impinging onto heated solid surfaces. The size and velocity of the secondary droplets is characterized making use of simultaneous image analysis and phase Doppler measurements to evaluate extended size distributions from 5.5μm up to a few millimetres. This procedure assured a consistent comparison of the results reported here with those previously reported in the literature, in similar experimental conditions. Although the study covers the various heat transfer regimes, particular attention is put on the phenomena occurring within the nucleate boiling regime, up to the critical heat flux temperature of the working fluids, as this is the upper boundary for the safe working conditions of many practical systems of interest, in the context of droplet/spray cooling.

The analysis focus on the physical description of the phenomena occurring at the liquid-solid interface to explain the triggering of the secondary atomization and leads to an empirical relation between the mean size of the secondary droplets and the dimensionless topographical parameter R_a/λ_R, which quantifies the relative magnitude of the high of the rough grooves with the distance between them. This relation seems to describe well the results that were uncorrelated in previous work, thus explaining the large discrepancies coming from experiments performed under apparently similar conditions, which are mainly introduced by surface topography.

1. Introduction

Secondary atomization at droplet/wall interactions has been addressed by several authors for impacts onto cold (*e.g.* Stow and Steiner, 1977, Mundo *et al.*, 1995, Gavaises *et al.*, 1996, Van der Wall *et al.* 2006) and heated targets (*e.g.* Naber and Farrel, 1993, Cossali *et al*., 2005, Akhtar and Yule, 2001, 2007a,b). For impacts onto cold surfaces, droplet disintegration and particularly the *prompt splash*, (i.e. the breakup occurring immediately after impact, as defined in Moita and Moreira, 2007 and more recently revisited in Pan *et al.*, 2010) is usually associated with the critical impact conditions (often the critical impact velocity) at which the inertial forces overcome surface tension and viscous forces: $\rho U_0^2 > \sigma_{lv} h_L / D_0^2$, where ρ and σ_{lv} stand for the liquid specific mass and surface tension, respectively, while D_0 and U_0 are the diameter and impact velocity of the primary droplets. h_L is the thickness of the lamella, which for an inertially dominated phenomenon is defined by the thickness of the viscous boundary layer, corresponding to the Stokes' first problem. Following Yarin and Weiss (1995) and the scaling performed as in Pasandideh-Fard *et al.* (1996), $h_L \sim (\nu D_0/U_0)^{1/2} = D_0 Re^{-1/2}$, where ν is the liquid kinematic viscosity.

For impacts onto heated surfaces different atomization mechanisms occur, at much smaller impact velocities and within a larger temporal scale, which are induced by thermal effects. The heat transfer phenomena lead to substantial morphological modifications of the spreading lamella, as a consequence of the temperature dependence of liquid properties and, ultimately, the disintegration occurs by disruption of the lamella by vapour pressure forces during liquid phase change. This is the so-called thermal induced atomization, which has been characterized by few authors such as Richter *et al.* (2005), Moreira *et al.*, (2007), Cossali *et al.*, (2008) and Muller *et al.* (2008). The characterization of the secondary atomization resulting from droplet/wall interactions is frequently

addressed in the context of the development of physical models to predict the number, size and velocity of the secondary droplets resulting from spray impingement. However, an accurate description and control of the physical processes involved in droplet disintegration is also vital in the practical design of many systems. For instance, few authors such as Bertola and Sefiane (2005) have recognized the need to control the thermal induced atomization in liquid cooling systems, while other, like Vukasinovic *et al.* (2004) have actually developed several artful strategies in the attempt of taking advantage the secondary atomization to endorse the performance of their cooling systems. However, the accurate description of the secondary atomization is a difficult goal which has not been achieved yet, mainly due to the co-existence of various dissimilar disintegration mechanisms, which depend on many parameters in a highly non-linear correlation. Among all the variables governing the secondary atomization mechanisms and particularly the thermal induced atomization, namely U_0, D_0, ρ, liquid properties, wettability and surface topography, the latter has been the most challenging to correlate. It is known that surface topography alters the wetting properties and consequently the dynamics of the spreading flow. In this context, several authors have been manufacturing customized rough surfaces (micro-patterned and/or with stochastic profiles) to alter their wettability and study its effect in the flow (*e.g.* Bico *et al.*, 2002, He *et al.*, 2003, Nakae *et al.*, 2005, Kannan and Sivakumar, 2007). Most of these works only deal with the spreading mechanism over non-heated surfaces.

The surface topography will also alter the heat transfer mechanisms. For instance, several authors such as Silk *et al.*, (2006), Hsieh and Yao, (2006), Sodke and Stephan (2007) and Shen *et al.*, (2010), report the enhancement of heat transfer during droplet and spray cooling when the impact surfaces are micro-textured with straight, cubic and pyramidal fins. However, the heat transfer phenomena occurring at droplet/spray impingement on structured surfaces are still quite scarcely studied, particularly for conditions including boiling regimes, for which the thermal induced atomization occurs. In this context, the present work addresses the study of the hydrodynamics and thermal response of the spreading lamella generated at the impact of single droplets on micro-structured surfaces. The mean diameter and velocity of the secondary droplets are analysed simultaneously with the thermal response of the primary droplet, which is related to the instantaneous surface temperature measurements performed within the liquid-solid interface region. The experimental conditions cover all the heat transfer regimes from single phase (non-boiling) to the film boiling regime, although with main emphasis in the nucleate boiling regime, up to the critical heat flux temperature, since this is the upper boundary for the safe working conditions of many practical systems of interest in the context of droplet/spray cooling. Furthermore, the main focus on this regime allows to improve the tuning of the correlations suggested in previous work (Moita and Moreira, 2009), mainly involving the dependency of the size of the secondary droplets with the topographic properties of the surfaces. These correlations are then interpreted to understand the effective limitations brought by the reduction in the residence time and area of the liquid mass in contact with the surface, as a non-negligible part of the primary drop is "taken away" from the surface by the ejected secondary droplets.

2. Experimental Approach

The experiments encompass the impact on individual droplets onto solid, dry surfaces accommodated on a copper base in which a 264 W cartridge heater is inserted. The surfaces are heated from room temperature up to 310ºC to cover the entire range of heat transfer regimes, from single phase evaporation to film boiling. The heat transfer regimes are identified based on the measurement of the surface temperature at droplet impact, which are complemented with visual inspection of the morphology of the spreading lamella. Additionally, the contact temperature, T_c determined as in Seki *et al.* (1978) - $T_c = [(\varepsilon_l T_l + \varepsilon_W T_W)/ (\varepsilon_l + \varepsilon_W)]$ is also evaluated to ensure that the behaviour of the different liquids is compared for similar superheating conditions. Here $\varepsilon = (\rho k C_p)^{1/2}$

is the thermal effusivity of the surface ε_w and of the liquid ε_l, while ρ, k and C_p stand for the specific mass, thermal conductivity and specific heat of the liquid, respectively. The critical heat flux (T_{CHF}) and, particularly the Leidenfrost temperatures ($T_{Leidenfrost}$) are evaluated for dynamic conditions, $U_0 \neq 0$, given their dependence on the properties of the system (surface properties and impact conditions).

Care is taken to assure that the surface is dry and recovers the initial temperature before the impact of the droplet. The liquid is kept in the droplet generator at room temperature and atmospheric pressure. Ambient temperature and relative humidity were measured through the experiments to ensure that their variation did not produce relevant changes in the results.

Although the rig allows varying the impaction angle, the present study focuses only on droplet impacts normal to the surface.

The analysis reported here is based on the experiments obtained with water and ethanol. These liquids were selected to study the effect of surface topography in the scenarios of partial and complete wetting, respectively. The significantly different thermophysical properties of these liquids will also lead to dissimilar fluid dynamic and heat transfer phenomena which also have to be considered in the general correlation describing the dependence of the thermal induced atomization with the topography of the surfaces. The properties of the liquids are shown in Table 1. These reference values, obtained at 25ºC, as well as their variation with temperature are taken from Özisik (1985), Incropera (1990) and Turns (1996).

Table 1. Thermophysical properties of the liquids. [a]From Tamura and Tanasawa (1959). [b]From Qiao and Chandra (1997).

Properties	Water	Ethanol
Surface tension $[Nm^{-1}]x10^3$	73.75	22.0
Specific mass $[kgm^{-3}]$	998	790
Kinematic viscosity $[m^2s^{-1}]x10^6$	1.0	1.4
Specific heat $[KJkgK^{-1}]$	4.18	2.44
Thermal conductivity $[Wm^{-1}K^{-1}]x10^3$	607.1	169
Latent heat of evaporation $[KJKg^{-1}]$	2272	846
T_{sat} [ºC]	100	78.3
$T_{Leidenfrost}$ [ºC] (nominal)	230[b]	182[a]

In this context, the impact conditions are varied to cover a broad range of of the most relevant dimensionless groups, (65<Weber number $We = \rho D_0 U_0^2 / \sigma_{lv}$ <1314; 170<Reynolds number $Re = U_0 D_0 / \nu$<11140; 2<Prandtl number $Pr = \nu C_p \rho / k$ <20, and 0.1<Jakob number $Ja = C_p (T_w - T_{sat}) / h_{fg}$ <1.9), which address the relative magnitude of the forces acting on the droplet. The Weber and the Reynolds numbers are based on the drop initial diameter and impact velocity. T_w and T_{sat} are the surface temperature and the saturation temperature of the liquid, respectively and h_{fg} is the latent heat of evaporation.

The working conditions are summarized in Table 2.

The surface temperature of the targets is monitored by thermocouples type K and managed by a PMA KS20-I temperature controller. One of the thermocouples is a fast response “Medtherm”

eroding-K-type which is embedded at the centre of the region where droplets impact. The signal of the thermocouples is sampled with a National Instruments DAQ board plus a BNC2120 and amplified with a gain of 300 before processing.

Table 2. Experimental conditions.

Liquid	D_0 [mm]	U_0 [ms^{-1}]	$T_{w,0}$ [ºC]
Water	2.8-3.0	0.4-3.1	25-310
Ethanol	2.2-2.4	0.4-2.5	25-260

Droplet impact is recorded by two synchronized high-speed cameras (a Kodak Motion Corder Analyzer, Series SR 512x420pixels, Model PS-120, with a maximum frame rate of 10kfps and a Phantom v4.2 from Vision Research Inc., with 512x512pixels@2100fps and a maximum frame rate of 90kfps), as in Moita and Moreira (2008), to provide both side and bottom view images of the spreading lamella. Transparent smooth glass surfaces heated by Joule effect from the back side with a transparent film of Indium Oxide, In_2O_3 were used to visualize the liquid-solid interface. The temperature of these glass surfaces is monitored by contact thermocouples of type K, which are positioned over the glass side. Deposition of the film is made by radio frequency (rf) plasma enhanced reactive thermal evaporation (rf-PERTE) at low substrate temperature (<100ºC). Details of the method and of the resulting relevant film properties are reported by Nunes de Carvalho *et al.* (2008). This deposition process allows obtaining a homogeneous film along the surface, as confirmed by scanning electron microscopy with x-ray microanalysis (SEM/EDS).

All the instrumentation is triggered by the same signal, emitted as the drop crosses a horizontal laser beam aligned with a photodiode.

2.1 Characterization of the surfaces

Surfaces of different materials and with diverse topographical characteristics were used to cover significantly different behaviour patterns of the impinging droplets. Wall effusivities, ε_w ranged from $7.2 \cdot 10^3 kg/Ks^{2.5}$, for stainless steel AISI316, to $14 \cdot 10^3 kg/Ks^{2.5}$ for aluminium surfaces.
The characterization of the surface topography naturally plays a crucial role. The amplitude of the rough peaks is quantified by the mean roughness, R_a, determined according to standard BS 1134 and by mean peak-to-valley roughness, R_z calculated according to standard DIN4768. The measurements are performed with an optical profile meter, (Surface Measuring System RM600-3D) which allows the 3D reconstitution of the surface topography. In fact, most of the rough surfaces are custom made, to have well defined topographical characteristics. The main geometrical properties of these micro-structured surfaces, defined as in Fig. are depicted in Table 3. The characterization of the "smooth" surfaces and/or with stochastic profiles is given in Table 4.

Each pair liquid-surface is also characterized by the equilibrium contact angles, θ, which were measured at room temperatures, inside a thermostatted ambient chamber (Ramé-Hart Inc., USA, model 100-07-00), using the Sessile Drop Method. For water drops deposited on the smooth stainless steel surfaces, θ_1=93.0º and θ_2=93.5º, while for the smooth glass surface ($R_a \approx 0\mu m$) used for visualization purposes, the contact angle with water is θ_4=38.5º. Complete wetting ($\theta \approx 0º$) is observed for all the surfaces when wetted by the ethanol droplets. The contact angle for the custom made surfaces varied between 85º and 121.5º with water droplets. Complete wetting ($\theta \approx 0º$) is observed for all the surfaces when wetted by the ethanol droplets.

A detailed description of the measurement procedures is presented in Moita and Moreira (2007).

Table 3. Main topographical characteristics of the micro-textured surfaces, which are made of copper, stainless steel, aluminium and silicon wafers.

Parameters	Range [μm]
a	10-500
l	20-500
h	1-500
λ_{R1}	16-500
λ_{R2}	16-500

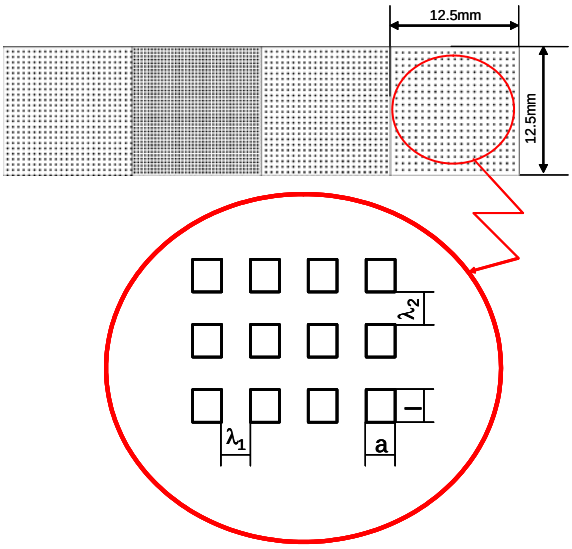

Fig. 1. Micro-textured surfaces: definition of the dimensions *a*, *l*, *h*, λ_{R1} and λ_{R2} characterizing the topography of the micro-textured surfaces taken at a sample of one of the masks used to produce the 32 textured surfaces. Each square of 12.5mmx12.5mm represents a different surface.

Table 4. Main topographical characteristics of "smooth" surfaces and/or with stochastic profiles.

Surface number	Surface Material	R_a [μm] ±10%	R_z [μm]
1	Stainless steel	0.31	2.32
2	Stainless steel	0.52	9.0
4	Glass	≈0	≈0

2.2 Measurement techniques

Large droplets (from 40μm up to a few millimetres) are evaluated from extensive post processing of the recorded images, while the size and velocity of small droplets, (2.5μm up to 250μm) are obtained from phase Doppler measurements. The probability density functions (PDF) obtained by each of the techniques are then combined to attain an extended-PDF, from which the mean size of the secondary droplets is evaluated as in Moreira *et al.* (2007). Temperature measurements taken during droplet impact allow complementing the study of fluid dynamics with the analysis of the heat transfer. For each experimental condition, the final temperature profile is averaged from 10 events, for similar impact conditions.

Regarding image processing, spatial resolution of the image acquisition system is 25μm, with 0.1ms of temporal resolution. The accuracy in the evaluation of the impact velocity U_0 is better than 3%, while for the droplet diameter D_0 is ±1.4%. The size distribution of large secondary droplets is obtained at several instants after impact. Fifty droplets, with similar D_0 and U_0 are taken for each experimental condition, so fifty images are analyzed per time step (i.e. for each time instant), to obtain statistically representative results. Time is made dimensionless with the initial droplet diameter and impact velocity, $\tau = t/(D_0/U_0)$. PDF's of drop diameters are then built at dimensionless time bins $\Delta\tau$=0.5, for $0 \leq \tau \leq 100$, which covers the most relevant period of droplet impact.

On the other hand, the phase Doppler instrument is a two-component system from Dantec. The optical configuration is summarized in Table 5, together with the main validation parameters.

A radial coordinate system is used as defined in Fig. 2, where r=0mm corresponds to the center of the impact region. Here, U and V stand, as usual, for the axial and radial velocity components, respectively. Positive values of the axial velocity U are taken downwards, in the direction of gravity, the same as for the impact velocity of the primary droplet U_0.

Table 5. Optical configuration of the phase Doppler instrument.

	Value
Transmitting optics	
Laser power [mW]	300
Wavelengths [nm]	514 and 488
Beam spacing [mm]	60
Transmitter focal length [mm]	310
Frequency shift [MHz]	40
Receiving optics	
Scattering angle [º]	70
Receiver focal length [mm]	310
Processor parameters	
U signal bandwidth [MHZ]	1.2
V signal bandwidth [MHZ]	0.4
S/N validation [dB]	0
Spherical validation [%]	10

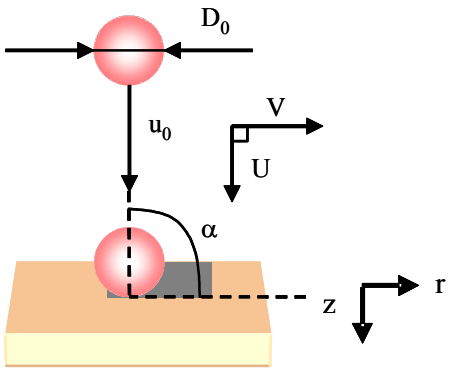

Fig.2. Radial system of coordinates used in the measurements with the phase Doppler instrument.

The measurement grid is selected from the spatial distributions obtained with the image analysis: measurements are reported at z=2.5 and z=5mm, above the surface and at radial coordinates r=0mm, r=3mm and r=6mm.

Several sources of inaccuracy affecting the phase Doppler measurements, *e.g.* low signal to noise ratio, for instance due to low intensity or light attenuation, the Gaussian distribution of light intensity in the effective measuring volume, multiple occurrence of droplets or size velocity correlation effects are well known to influence amplitude dependent quantities and were already discussed in Moita and Moreira (2009). Another relevant issue is related to the phase-diameter relation, which depends on the refractive index, for the refraction mode. With the present configuration, inaccuracy of the size measurements related to this issue is better than 7% (Moita and Moreira, 2009).

The processing procedure is then identical to that performed in the image analysis: the validated measurements are distributed in bins of dimensionless time $\Delta\tau$=0.5 for $0\leq\tau\leq100$. Finally, it is necessary to integrate the PDA measurements in time and in space, to have them statistically closer to those obtained by the image analysis. A uniform spatial distribution of the droplets is considered even for impacts onto tilted surfaces, based on the distributions obtained by image analysis. The size distributions obtained by each technique are then scaled by equating the count values within the overlapped size range, between 40μm and 250μm, by means of a least square method. Fig. 3 exemplifies the integrated construction of the size distribution of the secondary droplets distributions within the extended size range. The data was obtained for a water droplet (D_0=2.8mm, U_0=2.5ms^{-1}) impacting onto a smooth stainless steel surface (R_a=0.311μm, R_z=2.32μm) within the transition boiling regime.

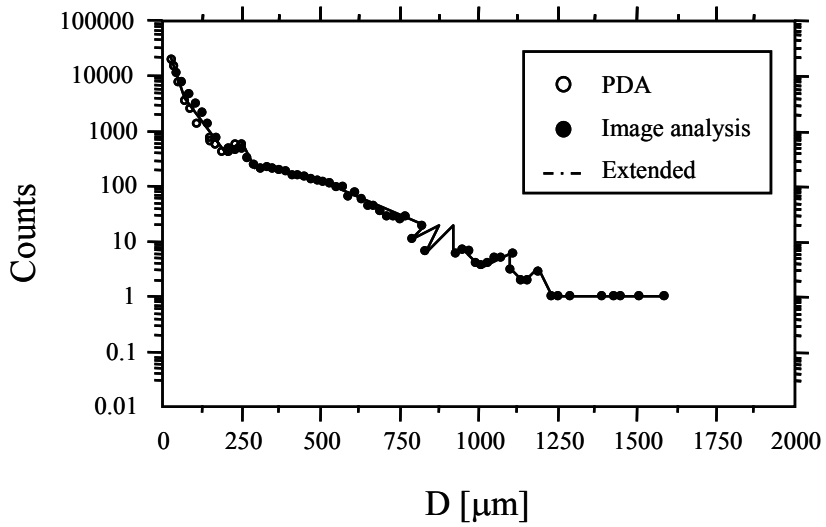

Fig. 3. Example of a reconstructed extended size distribution.

Afterwards, the mean and Sauter mean diameters are evaluated from the extended-PDF along the dimensionless time. Fig. 4 exemplifies the temporal evolution of the mean diameter obtained by the various techniques.

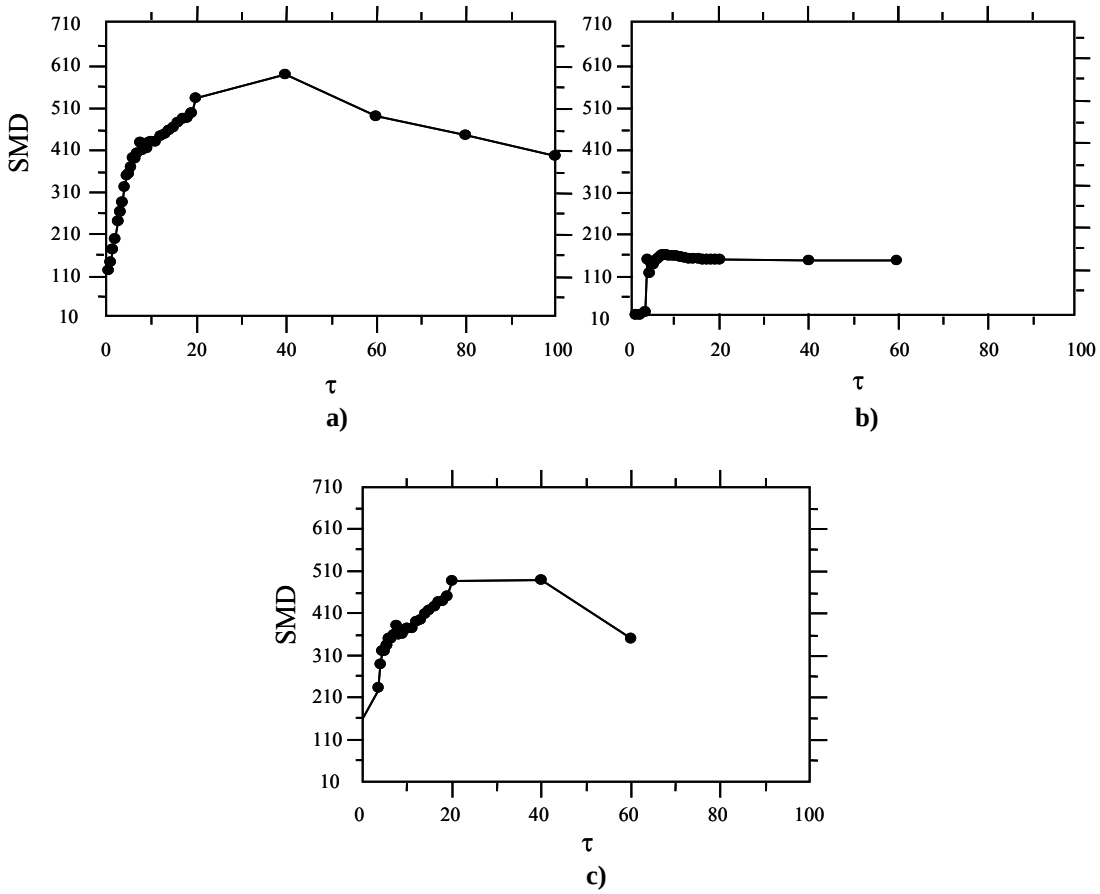

Fig. 4. Temporal evolution of the Sauter Mean Diameter of the secondary droplets generated from a water droplet (D_0=2.8mm, U_0=2.5ms^{-1}) impacting onto a stainless steel surface (R_a=0.311μm, R_z=2.32μm, α=90º), within the transition boiling regime. a) Image analysis processing; b) integrated phase Doppler measurements; c) extended-PDF.

3. Results and Discussion

Droplet dynamics at impact onto heated surfaces is known to be strongly dependent on the heat transfer regime. Previous research conducted by the authors provided the quantitative and qualitative description of the disintegration mechanisms thermally induced within the several heat transfer regimes. For drop impacts within the film boiling regime, a close observation to the morphology of the spreading lamella, based on the sequence of images recorded by the two synchronized high-speed cameras, showing both side and bottom (i.e. at the liquid-solid interface) views allowed to identify the co-existence of two disintegration mechanisms: the prompt disintegration of the rim, occurring within the first instants after impact, ($\tau<1$) and a strong complete disintegration of the lamella into large droplets, usually observed at later stages after impact, just before the complete levitation of the lamella (at $5<\tau<6.5$). The latter mechanisms is attributed to the disruption of the liquid ligaments of the cellular structures formed during spreading (between $1.3<\tau<5$). Following a dimensionless analysis of the parameters governing these mechanisms, the extended time averaged size of secondary droplets was well described by the correlation:

$$SMD/D_0=f(We, Re) \sim A_1 We_N^{-0.6} Re^{-0.23} \quad (1)$$

On the other hand, the triggering of the thermal induced atomization resulting from droplet impacts within the nucleate boiling regime is strongly related with the competitive relation between

the vapour pressure forces and surface tension forces. The size of the secondary droplets can be correlated with the impact conditions and with the liquid properties through the correlation:

$$SMD / D_0 = f(We, \mathrm{Re}, Ja) \sim A_2 We_N^{-0.14}\ \mathrm{Re}^{-0.11}\ Ja^{-0.3} \tag{2}$$

which gathers the dimensionless numbers expressing the forces acting onto the droplets. However, an evident correlation could not be devised yet to include the topographical characteristics of the surface. This is evident in the discrepancy of the experimental results reported by different authors in apparently similar conditions. Such discrepancy is illustrated in Fig. 5, which compares the results predicted by the empirical correlation (2) with those measured by Cossali *et al.* (2008) and Moita and Moreira (2009). The Figure clearly shows that droplets impacting with similar conditions (D_0=2.8mm, U_0=1.3ms^{-1}) generate secondary droplets with dissimilar mean sizes, depending on the topographical characteristics.

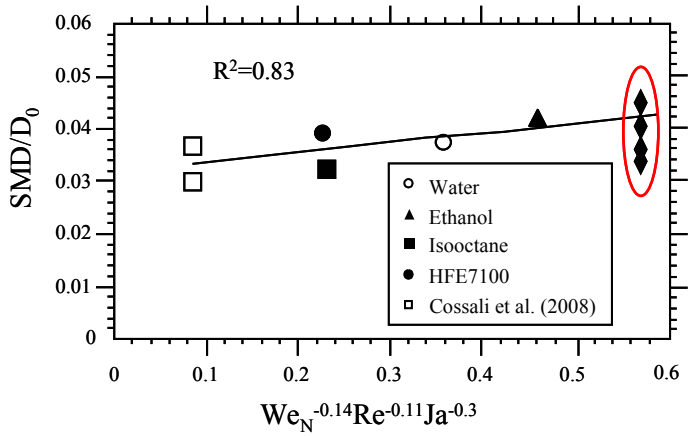

Fig. 5. Effects of surface topography on the size of secondary droplets generated by thermal induced atomization, within the nucleate boiling regime, for droplets impacting onto smooth surfaces. ($T_{contact,water}$= 141ºC, $T_{contact,isooctane}$= 140ºC, $T_{contact,ethanol}$= 110ºC, $T_{contact,HFE7100}$=102ºC). The degree of superheating, from the contact temperature is similar in both liquids ≅40ºC. The scattering caused by the non-scaled effect of the surface topography is highlighted by the elliptical line.

When analyzing the spreading behaviour of liquid droplets with significantly different liquid properties (*e.g.* water and ethanol) there are obvious morphological features which contribute to the particular thermal induced atomization of each liquid. The modification of the surface properties can alter this behaviour. The modifications introduced by the use of different roughness patterns are discussed in the following paragraphs, to understand the parameters that can be used to describe the size of the ejected droplets. The dynamic and thermal behaviour of water and ethanol droplets are compared to cover the distinct scenarios (hydrophobicity/partial wetting/complete wetting) which are usually addressed and modeled in these studies (*e.g.* Plawsky *et al.*, 2008).

Fig. 6 presents the simultaneous analysis of the thermal induced atomization during the impact of water and ethanol droplets and the subsequent thermal response based on the instantaneous measurements of the surface temperature within the liquid-solid interfacial region.

The results presented in this Figure are generated from droplet impacts at distinct velocities on a smooth stainless steel surface, within the nucleate boiling regime at similar overheating conditions.

The instantaneous surface temperature falls suddenly as the droplet contacts the surface, given the fast heat transfer occurring from the heated surface to the liquid, which is initially at room temperature. The higher thermal conductivity and specific heat of the water leads to the larger temperature descent when the droplet contacts the surface.

This scenario provides good conditions for surface rewetting for the water, given the high surface tension of this liquid.

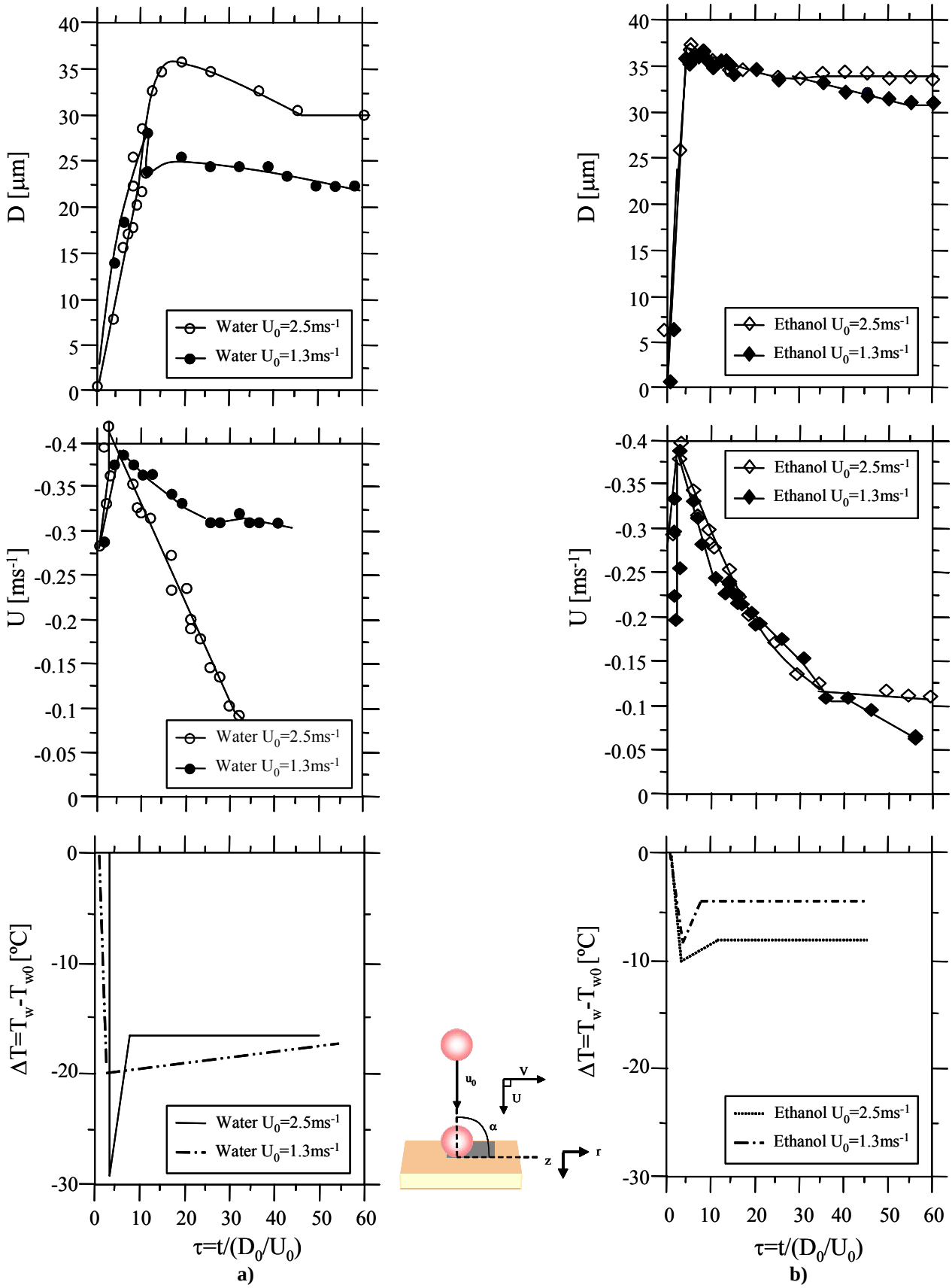

Fig. 6. Simultaneous measurements of the secondary atomization induced at droplet impact within the nucleate boiling regime and corresponding instantaneous surface temperature measured at r=0mm. The mean size and velocity (being U the axial component) of the secondary droplets are obtained by PDA measurements taken at r=0mm and z=5mm. The primary droplets of: a) a water droplet (D_0=2.8mm) and b) an ethanol droplet (D_0=2.4mm) impact on a smooth stainless steel surface (R_a=0.311µm, R_z=2.32µm). $AT_0=Tw_0-T_{sat}$=20ºC.

Additionally, the large latent heat of evaporation keeps the temperature low which is kept nearly constant during liquid evaporation. Consequently all the boiling process is delayed. Also, the higher surface tension of this liquid constrains for longer the vapour pressure forces, furhter delaying the disruption of the free surface of the lamella and therefore the thermal induced atomization, so the peak in the temporal evolution of the mean size of the secondary droplets (corresponding to the intense boiling period) occurs quite late after the droplet impact. A nearly opposite behaviour is observed for the ethanol droplets. The surface temperature decay is much smaller and the association of effects previously described for the water droplet acts to favour a fast boiling with subsequent promotion of the thermal induced atomization to occur at earlier instants after droplet impact. The force balance acting on the droplet for such low values of k, C_p, h_{fg} and σ_{lv} also produces a number of morphological features in the lamella of these liquids (*e.g.* the formation of cellular structures due to surface temperature gradients, as in Moita and Moreira, 2008) which will favor the fast evaporation and disruption of the lamella, further promoting the secondary atomization and decreasing the contact area and residence time of the liquid over the surface.

Both dynamic and thermal response of water and ethanol droplets are faintly affected by the impact conditions, as observed by the identical trend of the curves obtained for impacts at different velocities. The effect of liquid surface tension is not so clear within this small range of secondary droplets measured with the Phase Doppler instrument within the nucleate boiling regime, but the analysis of the extended droplet sizes shows that liquids with larger surface tension tend to give rise to smaller secondary droplets (*e.g.* Moreira *et al.* 2007, Moita and Moreira 2009).

The micro-textured surfaces are used to act in these phenomena at different levels, namely to increase the contact line length thus augmenting the spreading area and improving heat flux (*e.g.* Sodke and Stephan, 2007), but also so modify the boiling morphology of the lamella by promoting nucleation and different growth rates and transport mechanisms of the vapour bubbles (*e.g.* Agrawal *et al.*, 2005, Rioboo *et al.*, 2009). However, care must be taken to assure that the chosen roughness pattern is not generating other effects such as unexpected hydrophobicity and/or promotion of dryout regions. Therefore choosing the adequate pattern is an optimization process which requires the quantification of the topographical characteristics using practical scaled quantities. In order to assess on the effect of customized micro-patterns and on the most practical quantities which could be used to correlate the observed phenomena with the topographical characteristics, the impact of water and ethanol droplets was studied for several micro-patterned surfaces, within the various heat transfer regimes. In line with the analysis performed so far, Fig. 7 depicts the temporal evolution of the mean size and velocity of the thermally induced secondary droplets together with the corresponding instantaneous surface temperature during the spreading of the lamella. The Figure shows the best fit results from the surfaces tested so far. The impact velocity was kept low (U_0=1.3ms^{-1}) to avoid *prompt splash*.

The results show a dissimilar trend for water and ethanol droplets, thus suggesting the occurrence of different wetting regimes. So, for the water droplets there is an evident change of behaviour when the ratio R_a/λ_R of the target surfaces is altered: the thermal induced atomization occurs earlier and gives rise to larger secondary droplets for the lowest value of R_a/λ_R. On the contrary, as the water droplets impact surfaces with the same (larger) value of R_a/λ_R, (although obtained by combination of different rough amplitudes and wavelengths) the thermal induced atomization mechanisms are delayed and generate smaller secondary droplets.

Such behaviour is consistent with the temperature profiles measured at the substrate during droplet interaction (the delay in the thermal response is due to the increasing of the thickness of the targets for this set of experiments. However both smooth and textured surfaces for this case have the same thickness, so one can compare them).

These results can be explained as in Nakae *et al.* (2005), by performing a local balance of the interfacial forces acting on the system liquid-droplet-vapour. Reminding the heterogeneous wetting regime, described by Cassie and Baxter (1944), for a given rough peak amplitude of h_R, there

should be a critical wavelength λ_{RC} at which the liquid will contact the rough valley.

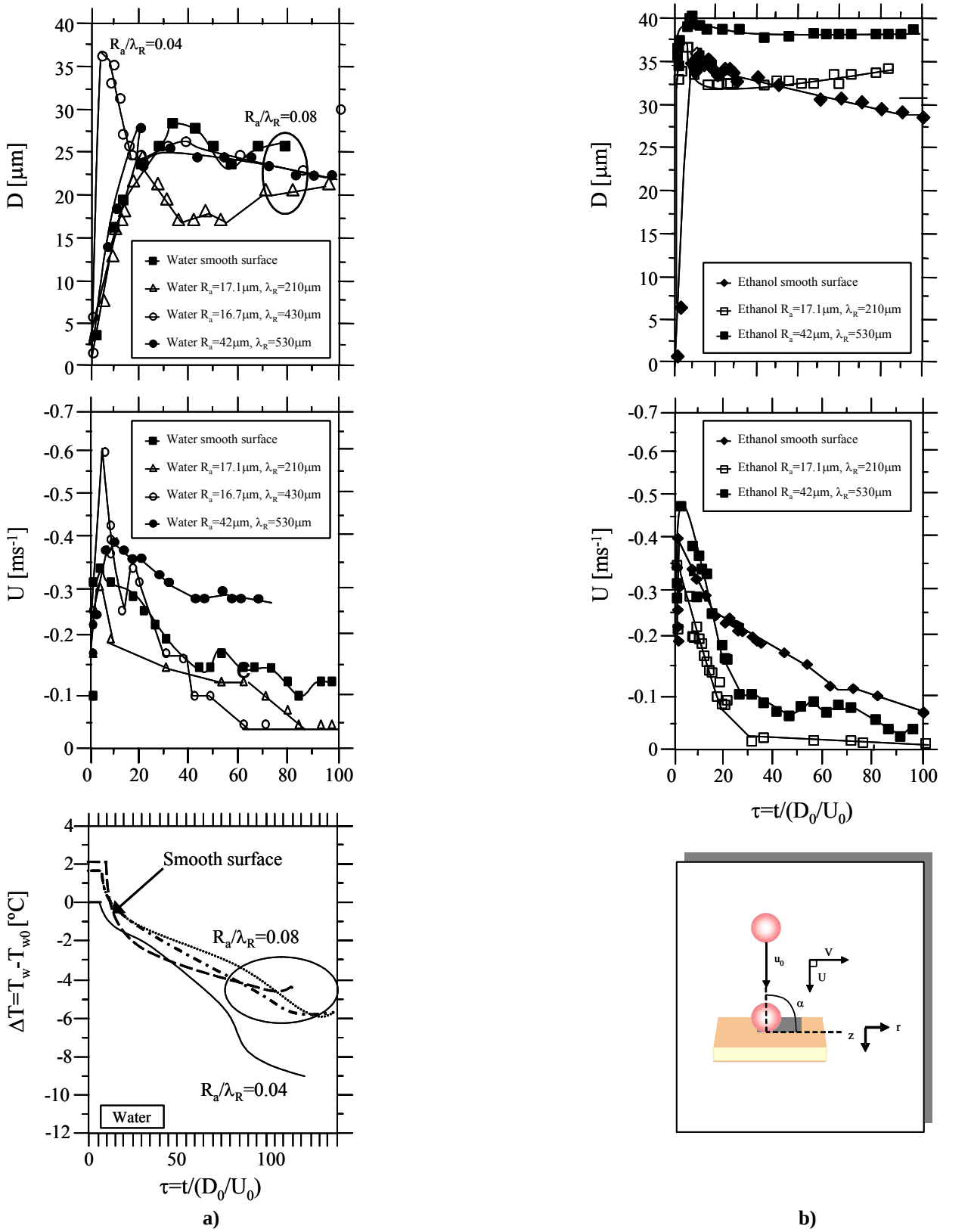

Fig. 7. Simultaneous measurements of the secondary atomization induced at droplet impact within the nucleate boiling regime and corresponding instantaneous surface temperature measured at r=0mm. The mean size and velocity (being U the axial component) of the secondary droplets are obtained by PDA measurements taken at r=0mm and z=5mm. The primary droplets impact of: a) a water droplet (D_0=2.8mm) and b) an ethanol droplet (D_0=2.4mm) on different micro-textured surfaces, within the nucleate boiling regime. $AT_0=Tw_0-T_{sat}$=40ºC.

This will occur for a consequent radius of curvature at the liquid-solid-interface. Alternatively, considering that the curvature of the liquid droplet in contact to the surface (sessile drop) is controlled by the Laplace equation:

$$\Delta p = \sigma_{lv}\left(\frac{1}{R_1}+\frac{1}{R_2}\right) \tag{3}$$

and assuming an almost axysymmetric radius at the liquid/vapour interface, the radius of curvature at the liquid solid interface can be estimated from:

$$\sigma_{lv}\left(\frac{1}{R_1}+\frac{1}{R_2}\right)=\frac{2\sigma_{lv}}{R_0}+gZ(\rho_l-\rho_v) \tag{4}$$

and

$$\frac{1}{R}=\frac{1}{R_0}+\frac{gZ(\rho_l-\rho_v)}{2\sigma_{lv}} \tag{5}$$

where Z_R is the absolute height from the substrate to the top and ρ_l and ρ_v are the specific mass of the liquid and vapour, respectively. The model derived from this approach was not easy to apply, since the shape of the rough asperities is more complex in the present work. Nevertheless, the values of the apparent contact angles with water, measured on the present surfaces ($85º<\theta<121.5º$) are similar to those determined in Nakae *et al.* (2005), so the values of the radius become similar. By introducing a relation between the intrinsic contact angle (the Young angle in Cassie and Baxter relation) and the roughness amplitude, Nakae *et al.* (2005) end to conclude a unique relation between the radius of curvature at liquid/solid/vapour interface R and the intrinsic contact angle. Further manipulation of the formulation, by taking into account that the maximum R is controlled by the Laplace equation allows deriving empirical correlations, for which $R=A\lambda_R-B$. From this analysis, it is possible to estimate a hydrophobic behaviour for the rough surfaces with the relation $R_a/\lambda_R=0.08$. So, for this ratio, the surfaces, when wetted by the water droplets become hydrophobic and the lamella spreads within a heterogeneous wetting regime, thus promoting the entrapment of air and vapour layers. On the other hand, the lower R_a/λ_R promotes the liquid-solid contact within a homogeneous wetting regime.

This effect is not so evident for the ethanol droplets for which the mean diameter of the secondary droplets increases as the roughness amplitude increases. In this case, the local force balance renders a homogeneous wetting behaviour for all the pattern combinations used in the present set of experiments. The surface with smaller rough amplitude and smaller λ_R is in the critical limit so the hydrodynamic behaviour is close to that observed for the smooth surface. However, care should be taken because for complete wetting systems the analysis is not exactly the same as that performed in Nakae *et al.*, 2005, since the capillarity effects govern most part of the spreading behaviour and one must analyse in specific quantities, the competition between the surface tension and the disjoining pressure in very thin films (*e.g.* Plawsky *et al.* 2009).

For the impact of ethanol droplets, surface enhancement increases the contact line and subsequently enhances the heat transfer occurring between the surface and the lamella. As a result, the mean size of the secondary droplets is larger and the thermal induced atomization is triggered quite early when compared to that of water droplets. Additionally, the thickness of the spreading lamella may remain larger, further contributing to the larger mean diameter of the secondary droplets.

From the discussion presented above, the ratio R_a/λ_R seems to be useful in correlating droplet

behaviour with the topography of the surfaces and, as depicted in Fig. 8, for the present set of experiments it can actually gather a number of results, obtained at similar impact conditions, which are quite scattered when related to several other quantities frequently used to characterize surface topography.

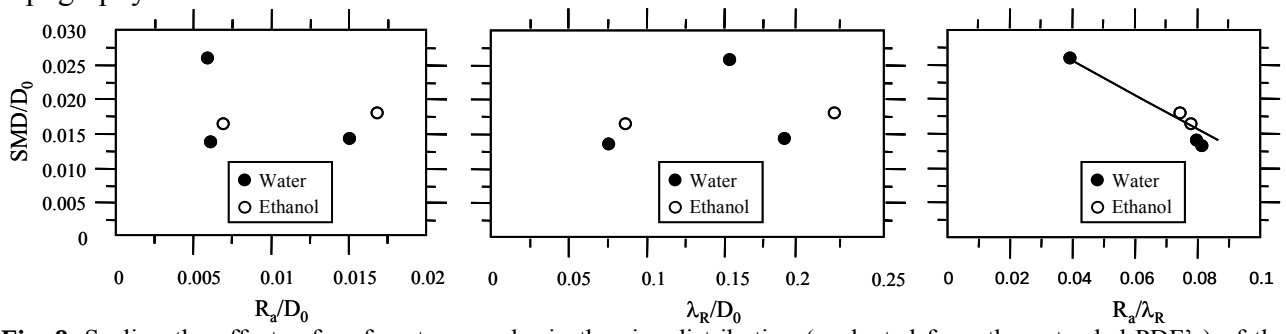

Fig. 8. Scaling the effects of surface topography in the size distribution (evaluated from the extended-PDF's) of the secondary droplets generated from thermal induced atomization, within the nucleate boiling regime. The primary droplets of water (D_0=2.8mm, U_0=1.3ms^{-1}) and ethanol (D_0=2.4mm, U_0=1.3ms^{-1}) are impacting onto textured stainless steel surfaces. Relation of the mean diameter of the secondary droplets with: a) the dimensionless roughness amplitude, b) the dimensionless fundamental wavelength, c) the ratio R_a/λ_R.

Although this ratio has been used in studies performed by other authors to analyse the heat transfer and the wetting behaviour (*e.g.* Amon *et al.*, 2005, Herminghaus *et al.*, 2008), thus reinforcing its potential, a final correlation requires further investigation and should include also geometrical relations for the shape of the grooves, as they can have a vital role in changing the wetting regime and is not expected to have such a linear relation. Nevertheless this type of relations is quite relevant in cooling applications because, from the mean size and number of the secondary droplets one may have control on the liquid mass that is taken away from the surface. This is important because although liquids like water have an overall better cooling performance, they may loose advantage for surfaces which are much hydrophobic (this can be easily evaluated from the surface temperature measurements and heat transfer calculations) but they can also loose advantage for the patterns rendering much vigorous thermal induced atomization (which generates larger droplets). In line with this, representations similar to that proposed in Fig 8c) can help to establish performance maps in the process of finding the optimum roughness pattern. The final optimum configuration is therefore a compromising solution of endorsing liquid-solid contact without promoting an excessively intense thermal induced atomization.

4. Final remarks

The present study encompasses the simultaneous analysis of the hydrodynamics and thermal response of the spreading lamella generated at the impact of single droplets on micro-structured surfaces. The mean diameter and velocity of the secondary droplets are evaluated from the combined use of high-speed image analysis with phase Doppler measurements, to cover an extended droplet size distribution, ranging from 5μm up to a few millimetres. These data are then analysed simultaneously with the thermal response of the primary droplet, which is related to the instantaneous surface temperature measurements performed within the liquid-solid interface region. The experimental conditions cover all the heat transfer regimes from single phase (non-boiling) to the film boiling regime, although with main emphasis in the nucleate boiling regime, up to the critical heat flux temperature, which is the upper boundary for the safe working conditions of many practical systems of interest in the context of droplet/spray cooling. Additionally, this procedure allowed to improve the tuning of the correlations suggested in previous work, mainly involving the dependency of the size of the secondary droplets with the topographic properties of the surfaces. The results obtained so far show a good correlation between the mean sizes of the secondary droplets generated by thermal induced atomization with the ratio R_a/λ_R, which allowed to gather a

number of results, obtained at similar impact conditions, which are quite scattered when related to several other quantities frequently used to characterize surface topography.

5. Acknowledgments

The authors acknowledge the contribution of the National Foundation of Science and Technology by supporting A. S. Moita with a Fellowship (Ref:SFRH/BPD/63788/2009) and by partially financing the research under the framework of project PTDC/EME-MFE/69459/2006.

References

Agrawal, A., Park, J., Ryu, D. Y., Hammond, P. T., Russel, T., Mckinley, G. H. (2005) Controlling the location and spatial extent of nanobubbles using hydrophobically nanopatterned surfaces. Nano Letters, 5(9):1751-1756.

Akhtar, S. W., Nasr, G.G., Yule, A. J. (2007a) Characteristics of water droplet impaction behaviour on a polished steel heated surface: Part I. Atom. & Sprays, 17(8):659-681.

Akhtar, S. W., Nasr, G.G., Yule, A. J. (2007b) Characteristics of water droplet impaction behaviour on a polished steel heated surface: Part II. Atom. & Sprays, 17(8):683-729.

Akhtar, S. W., Yule, A. J. (2001) Droplet impaction on a heated surface at high Weber numbers. Proc. ILASS-Europe 2001, Zurich, Switzerland.

Amon, C. H., Yao, S.-C., Hsieh, C.-C. (2005) Microelectromechanical system-based evaporative thermal management of heat flux electronics. Transactions of the ASME, 127:66-75.

Bertola, V., Sefiane, K. (2005) Controlling secondary atomization during drop impact on hot surfaces by polymer additives, Phys. Fluids, 17, 108104.

Bico, J., Thiele, U., Quéré, D. (2002) Wetting of textured surfaces, Coll. Surf. A Physicochem.Eng. Aspects, 206:41-46.

Cassie, A. B., Baxter, S. (1944) Wettability of porous surfaces. Trans. Faraday Soc., 40:546-551.

Cossali, G. E., Marengo, M., Santini, M. (2005) Secondary atomization produced by single drop vertical impacts onto heated surfaces. Exp. Thermal Fluid Sci., 29:973-946.

Cossali, G. E., Marengo, M., Santini, M. (2008) Thermally induced secondary atomization produced by single drop impact onto heated surfaces. Int. J. Heat Fluid Flow, 29(1):167-177.

Gavaises, M. Theodorakakos, A., Bergeles, G. (1996) Modeling wall impaction of Diesel sprays. Int. J. Heat Fluid Flow, 17(2):130-138.

He, B., Neelesh, Patankar, A., Lee, J. (2003) Multiple equilibrium droplet shapes and design criterions for rough hydrophobic surfaces. Languir2003, 19:4999-5003.

Herminghaus, S., Brinkmann, M., Seemann, R. (2008) Wetting and dewetting of complex surface geometries. Annu. Rev. Mater. Res., 38:101-121.

Hsieh, C.-C., Yao, S.-C. (2006) Evaporative heat transfer characteristics of a water spray on micro-structured silicon surfaces. Int. J. H. Mass Transf., 49:962-974.

Incropera, F. P., DeWitt, D. P. (1990) Fundamentals of heat and mass transfer, 3rd Ed., John Wiley & Sons.

Kannan, R., Sivakumar, D. (2007) Impact of liquid drops on a rough surface comprising microgrooves. Exp. Fluids, 44(6):927-938.

Moita, A. S., Moreira, A. L. N. (2007) Drop impacts onto cold and heated rigid surfaces: morphological comparisons, disintegration limits and secondary atomization. Int. J. Heat Fluid Flow, 28:735-752.

Moita, A. S., Moreira, A. L. N. (2008) Boiling morphology and heat removal of impinging coolant droplets. Proc. 22nd ILASS-2008, Como Lake, Italy.

Moita, A. S., Moreira, A. L. N. (2009) Development of empirical correlations to predict the secondary droplet size of impacting droplets onto heated surfaces. Exp. Fluids, 47:755-768.

Moreira, A. L. N., Moita, A. S., Cossali, G. E., Marengo, M., Santini, M. (2007) Secondary atomization of water and isooctane drops impinging onto tilted heated surfaces. Exp. Fluids, 43:297-313.

Muller, A. Dullenkopf, K., Bauer, H.-J. (2008) Analysis of droplet wall interactions with graded surface roughness. Proc. 22nd ILASS-2008, Como Lake, Italy.

Mundo, C.H.R, Sommerfeld, M., Tropea, C. (1995) Droplet-wall collisions: experimental studies of the deformation and break-up processes. Int. J. Multiphase Flow, 21(2): 151-173.

Naber, J. D., Farrel, P. (1993) Hydrodynamics of droplet impingement on a heated surface. SAE Paper 930919.

Nunes de Carvalho, C., Lavareda, G., Parreira, P., Amaral, A. Botelho do Rego, A. M. (2008) Influence of oxygen partial pressure on the properties of undoped InOx films deposited at room temperature by rf-PERTE. J. Non-Crystalline Solids, 354(15-16):1643-1647.

Özisik , M. N. (1985) Heat Transfer: a basic approach, Mc-Graw Hill.

Pan, K.-L., Tseng, K.-C., Wang, C.-H. (2010) Breakup of a droplet at high velocity impacting a solid surface. Exp. Fluids, 48:143-156.

Pasandideh-Fard, M., Qiao, Y. M., Chandra, S., Mostaghimi, J. (1996) Capillary effects during droplet impact on a solid surface. Phys. Fluids, 8(3):650-658.

Plawsky, J. L., Ojha, M., Chatterjee, A., Wayner, P. C. Jr. (2008) Review of the effects of surface topography, surface chemistry and fluid physics on evaporation at the contact line. Chem. Eng. Comm, 196:658-696.

Qiao, Y. M., Chandra, S. (1997) Experiments on adding a surfactant to water drops boiling on a hot surface. Proc. Royal Soc. London A, 453:673-689.

Richter, B., Dullenkopf, K., Bauer, H.-J. (2005) Investigation of secondary droplet characteristics produced by an isooctane drop chain impact onto a heated piston surface. Exp. Fluids 39:351-363.

Rioboo, R., Marengo, M., Dall'Olio, S., Voue, M., De Coninck, J. (2009) An innovative method to control the incipient flow boiling through Grafted surface with chemical patterns. Langmuir Letter, Langmuir 2009, 25(11):6005-6009.

Seki, M, Kawamura, H, Sanokawa, K. (1978) Transient temperature profile of a hot wall due to an impinging liquid droplet. J. Heat Transf., 100:167-169.

Shen, J., Graber, C., Liburdy, J., Pence, D., Narayanan, V. (2010) Simultaneous droplet impinging dynamics and heat transfer on nano-structured surfaces. Exp. Thermal Fluid Sci., 34:496-503.

Silk, E. A., Kim, J., Kiger, K. (2006) Spray cooling of enhanced surfaces: impact of structured geometry and spray axis inclination. Int. J. H. Mass Transf., 49:4910-4920.

Sodke, C., Stephan, O. (2007) Spray cooling on micro-structured surfaces. Int. J. H. Mass Transf., 50:4089-4097

Stow, C. D., Stainer, R. D. (1977) The physical products of a splashing water drop. J. Met. Soc. Japan, 55:518-531.

Tamura, Z., Tanasawa, Y. (1959) Evaporation and combustion of a drop contacting with a hot surface. 7th Symp. (Int.) Combustion, Buttertvorths, London, p. 509-522.

Turns, S. R. (1996) An introduction to combustion: concepts and applications, McGraw-Hill.

Vander Wall, R. L. G., Berger, G. M., Mozes, S. D. (2006) The combined influence of a rough surface and thin fluid film upon the splashing threshold and splash dynamics of a droplet impacting onto them. Exp. Fluids, 40:23-32.

Vukasinovic, B., Smith, M. K., Glezer, A. (2004) Spray characterization during vibration induced drop atomization. Phys. Fluids, 16(2):396-405.

Yarin, A. L., Weiss, D. A. (1995) Impact of drops on solid surfaces: self-similar capillary waves and splashing as a new type of kinematic discontinuity. J. Fluid Mech., 283:141-173.